



Fabrication of a Flexible Aqueous Textile Zinc-Ion Battery in a Single Fabric Layer

Sheng Yong^{1*}, Nicholas Hillier² and Stephen Beeby¹

¹Center for Flexible Electronics and E-Textiles, School of Electronics and Computer Science, University of Southampton, Southampton, United Kingdom, ²Energy Storage and Its Applications Centre of Doctoral Training, University of Southampton, Southampton, United Kingdom

Zinc-ion batteries (ZIB), with various manganese oxide-based cathodes, provide a promising solution for textile-based flexible energy storage devices. This paper demonstrates, for the first time, a flexible aqueous ZIB with manganese-based cathode fabricated in a single woven polyester cotton textile. The textile was functionalized with a flexible polymer membrane layer that fills the gaps between textile yarns, enabling fine control over the depth of penetration of the spray deposited manganese oxide cathode and zinc anode. This leaves an uncoated region in the textile-polymer network that acts as the battery's separator. The textile battery cell was vacuum impregnated with the aqueous electrolyte, achieving good wettability of the electrodes with the electrolyte. Additionally, the choice of cathodic material and its influence over the electrochemical performance of the zinc ion battery was investigated with commercially available Manganese (IV) oxide and Manganese (II, III) oxide. The textile ZIB with Manganese (II, III) oxide cathode (10.9 mAh g^{-1} or $35.6 \mu\text{Ah cm}^{-2}$) achieved better performance than the textile ZIB with Manganese (IV) oxide (8.95 mAh g^{-1} or $24.2 \mu\text{Ah cm}^{-2}$) at 1 mA cm^{-2} (0.3 A g^{-1}). This work presents a novel all-textile battery architecture and demonstrates the capability of using manganese oxides as cathodes for a full textile-based flexible aqueous ZIB.

Keywords: wearable technology, e-textile, energy storage, electrochemical energy storage, textile battery, zinc-ion battery and polymer membrane

INTRODUCTION

In recent years, the combination of electronic functionality within fabric materials has spawned the electronic textiles (e-textiles or smart fabrics) research domain. Now, complex flexible electronic devices and systems can be realized on, or within, textile substrates (Wicaksono et al., 2020; Komolafe et al., 2021), and have found use in wearable applications such as consumer electronics (Fromme et al., 2021), healthcare monitoring (Yao et al., 2021; Lahmann et al., 2022) and light-emitting display (Cinquino et al., 2021; Shi et al., 2021). E-textiles also exploit enabling-technologies such as wireless sensing (Somov et al., 2017), data transmission (Atalay et al., 2019), programmable logic array (Cleary et al., 2021) and flexible circuits (Komolafe et al., 2019). These systems all require a power supply to meet their electrical energy demands and this is typically achieved using conventional rigid batteries (Peppler and Glosson, 2013; Mauriello et al., 2014). Such batteries are impractical to use and are incompatible with the flexible properties and feel of a fabric material. The emergence of e-textile systems has therefore driven the requirements for high performance, flexible, reliable and durable textile-based energy storage devices that can replace the conventional battery.

OPEN ACCESS

Edited by:

Jegatha Nambi Krishnan,
BITS Pilani K K Birla Goa Campus,
India

Reviewed by:

Mihai Duduta,
University of Toronto, Canada
Zining Yang,
University of Illinois at Urbana-
Champaign, United States

*Correspondence:

Sheng Yong
s.yong@soton.ac.uk

Specialty section:

This article was submitted to
Wearable Electronics,
a section of the journal
Frontiers in Electronics

Received: 31 January 2022

Accepted: 09 May 2022

Published: 06 June 2022

Citation:

Yong S, Hillier N and Beeby S (2022)
Fabrication of a Flexible Aqueous
Textile Zinc-Ion Battery in a Single
Fabric Layer.
Front. Electron. 3:866527.
doi: 10.3389/felec.2022.866527

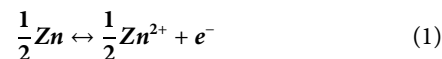
Previously, energy storage devices such as supercapacitors and lithium-ion batteries have been successfully demonstrated with textile substrates, fabricated using solution-based chemistries and standard manufacturing processes familiar to the textile industry. Yong et al (Yong et al., 2018) implemented a solid-state supercapacitor in a single cotton fabric layer. This device was made with spray coated carbon electrodes, whose thickness was controlled by precisely modifying the fabrication process and ink properties. This left an uncoated textile region at the center of the cotton, forming the device's separator and gel electrolyte holder. The flexible device achieved a specific capacitance of 49 mF cm^{-2} but the suitability of the process for different textiles depends upon the fabric thickness and properties such as wettability and absorption. While non-hazardous textile supercapacitors compatible with e-textile systems can be readily fabricated, their poor energy density and high leakage current impedes their use as a practical power supply for e-textile devices and systems (Zhao and Burke, 2021). In comparison with the supercapacitor, lithium-ion batteries can store and supply much higher levels of electrical energy, but their inherent inflexibility (Chen et al., 2021), safety concerns (Wu et al., 2019) and cost are limiting their practical application in e-textile systems. Pu *et al.* (Pu et al., 2015) demonstrated a lithium-ion battery with a conductive nickel coated fabric used as the current collector. Both cathode (LiFePO_4) and anode ($\text{Li}_4\text{Ti}_5\text{O}_{12}$) were doctor bladed and cured on top of the nickel coated cloth. The textile based flexible lithium-ion battery was then encapsulated within an aluminum pouch with a discrete separator and the electrolyte (1 M LiPF_6 in EC: DMC). This device achieved a capacity of 81 mAh g^{-1} but whilst it uses textile substrates it is essentially a separate discrete battery with limited flexibility.

Yarn shaped supercapacitors (Wu et al., 2019) and lithium-ion batteries (Qlan et al., 2020) are also compatible with e-textiles. Such functional yarns can be woven, knitted or embroidered within the textile. Yarn based solutions are restricted to materials that can be coated directly on the fibers and reliably fabricating such devices is challenging, with parameters such as increasing resistance with length degrading the specific performance and/or reducing repeatability (Fakharuddin et al., 2021; Wang S. et al., 2022). The balance between electrochemical performance and the safety and practicality of devices are important for wearable e-textiles energy storage. A practical energy storage solution must be reliable, safe and robust, being able to withstand both mechanical impacts, compressive squeezing and being folded as well as surviving machine wash cycles and exposure to detergents. Realising lightweight, rechargeable, flexible, robust, and effectively sealed textile-based energy storage devices remains an ongoing research challenge.

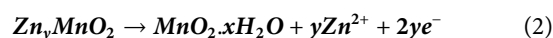
In comparison with lithium-ion battery zinc-ion batteries (ZIBs) with a mildly acidic or neutral aqueous electrolyte are a potential rechargeable electrochemical energy storage solution suitable for e-textile applications. Rechargeable aqueous ZIBs are less hazardous for the environment, safer, inherently more flexible and less expensive than lithium-ion batteries, with sufficient capacity and energy density to power e-textile systems (Selvakumaran et al., 2019). In addition, the assembly

of ZIBs can be done in air, offering reduced fabrication complexity. A ZIB typically consists of a zinc metal anode, a porous separator with a low hazard electrolyte and various metal oxides such as V_2O_5 (Javed et al., 2020), ZnMn_2O_4 (Sun et al., 2017), manganese (IV) oxide (MnO_2) [Jiao et al., 2020] and manganese (II, III) oxide (Mn_3O_4) (Hao et al., 2018)] as the cathode. The metal zinc anode has a high theoretical capacity of 820 mAh g^{-1} (Wang F. et al., 2018). ZIBs use zinc ions as the charge carriers and the MnO_2 cathode and its reaction formulas with an aqueous zinc sulfate electrolyte can be expressed as Eqs 1–4 (Sun et al., 2018):

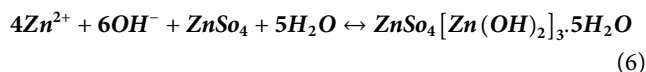
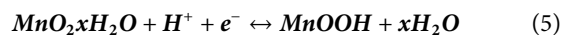
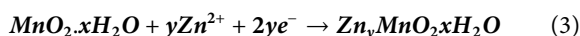
Anode:



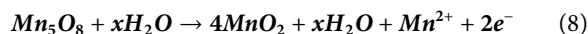
Cathode (during charge):



Cathode (during discharge):



In an aqueous ZIB cell with a Mn_3O_4 the cathode, Mn_3O_4 transforms into MnO_2 (ϵ phase) (Wang L. et al., 2018). This improves the long-term cycling stability and provides an efficient and effective approach for ZIB operation (Zhao et al., 2020), the reaction formulas for the initial charging cycle being expressed as Eqs 7, 8 (Zhao et al., 2020):



The implementation of ZIBs within a textile or using textile like substrates (e.g., woven stainless steel mesh) with manganese oxides has been demonstrated. Huang *et al.* (Huang et al., 2019) implemented a ZIB with a zinc metal anode and MnO_2 cathode. The anode was realized by electrodepositing zinc onto carbon cloth, the cathode was prepared with MnO_2 and reduced graphene oxide as a conductive additive vacuum filtrated through the textile. The flexible ZIB was assembled with an additional rice paper separator and characterized in an open-air environment using a zinc sulfate/manganese sulfate hydrogel electrolyte. This device demonstrated a specific capacity of 291.5 mAh g^{-1} at a discharge current of 0.15 A g^{-1} (based on a mass loading of MnO_2 of 17.75 mg cm^{-2}). Chen *et al.* (Chen et al., 2020) demonstrated a ZIB based on porous, cube-like, Mn_3O_4 /carbon composite cathode and a zinc metal anode. The Mn_3O_4 /carbon composite was synthesized with potassium permanganate and glucose in deionized water through a hydrothermal process, which was then coated on a stainless-steel mesh to form the cathode. The ZIB was assembled and tested in a coin battery test cell (CR 2032) with a paper separator and a zinc sulfate/manganese sulfate aqueous electrolyte. This demonstrated a

specific capacity of 323.2 mAh g^{-1} at a discharge current of 0.1 A g^{-1} . In both cases, the batteries were assembled in a multiple layer structure, using specially engineered textiles or a metal mesh and combined with a discrete filter paper layer as the separator. The use of a discrete filter paper layer in textile ZIB design requires all three material layers to be assembled in a rigid package such as metal coin cell or pouch. These packages are convenient for testing and to protect the device but limit any flexibility offered by the textiles-based electrodes.

In addition to filter paper separators, previous ZIBs have also been demonstrated with a discrete polymer-based porous separators such as polyethylene oxide (PEO) (Jin et al., 2020) and polyacrylonitrile (PAN) (Lee et al., 2018). Generally, polymer-based separators have been applied in ZIB designs as a replacement for the filter paper separator and result in improved cycling stability (Wang et al., 2021), battery efficiency (Zhao et al., 2018) and overall safety (Liu et al., 2018). Potential issues with the polymer separators including low film ionic conductivity, degradation when exposed to the ambient environment and, with respect to textile-based batteries, the adhesion between the polymer separator and textile has not been investigated. Examples of batteries with the polymer separators have been assembled as multilayer structures and were packaged in a coin cell. These works identify a potentially textile compatible approach for achieving a fabric-based separator and such a porous, chemically and mechanically stable polymer separator would be highly beneficial for textile battery design (Zhang et al., 2018; Jang et al., 2020). The benefits of such a textile integrated separator have already been demonstrated in a supercapacitor (Yong et al., 2019). In this work, a co-polymer porous membrane was first printed on and absorbed into a polyester cotton followed by a phase inversion process. The co-polymer membrane was formed from a mixture of ethylene-vinyl acetate (EVA) and poly-methyl methacrylate (PMMA) and this membrane together with textile yarns was used as the separator for supercapacitor. The activated carbon electrodes were then spray coated onto both sides of the polyester cotton textile with the level of impregnation being controlled by porous membrane. The encapsulated flexible supercapacitor demonstrated an areal capacitance of 20.6 mF cm^{-2} .

In this paper, we report for the first time an approach for fabricating a flexible ZIB cell that exploits the porous polymer separator enabling the zinc anode and manganese based cathode to be fabricated on a single textile layer and combined with an aqueous electrolyte. Combining the structure of the textile with the co-polymer porous membrane produces an elegant solution that avoids the need for a multilayer structure. The device is entirely solution processed with the battery's cathode and anode being fabricated by spray coating zinc and manganese oxide inks on to the top and bottom surfaces of the textile substrates. These inks were made using commercially available zinc, amorphous manganese (IV) oxide and manganese (II, III) oxide powders mixed with carbon black and an EVA binder. The flexible textile battery was fully saturated with a zinc sulphate and manganese sulphate aqueous electrolyte and tested with a nickel infused stainless steel film as the top/bottom current collector in order to study its energy storage characteristics.

EXPERIMENTAL SECTION

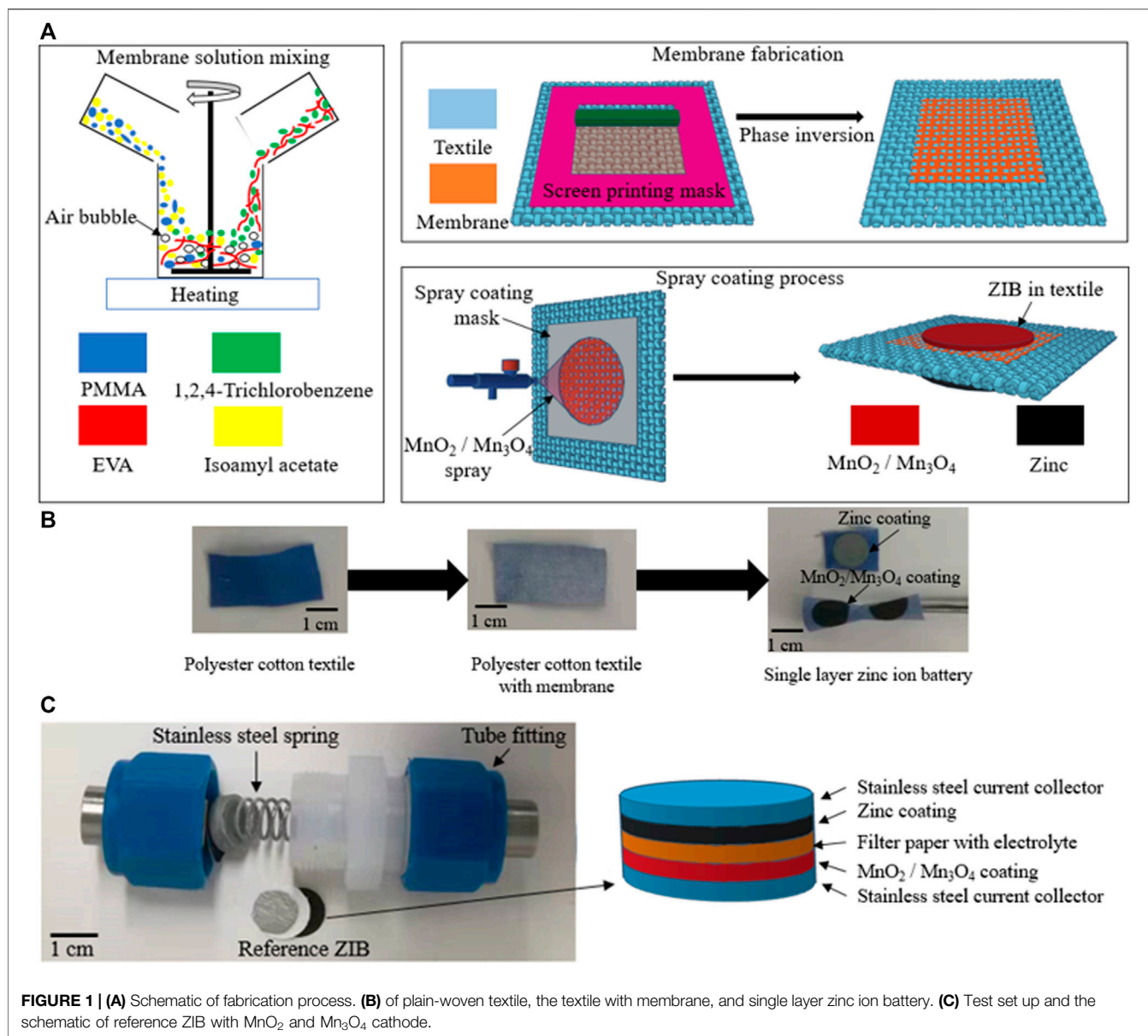
Materials

EVA beads (vinyl acetate 25 wt. % and 40 wt. %), used for the electrode ink and membrane respectively, PMMA powder ($M_w = 120,000 \text{ g/mol}$), amorphous manganese (IV) oxide, amorphous manganese (II, III) oxide powder (97% purity), zinc powder (99.9% purity), carbon nano-powder additive ($<100 \text{ nm}$ particle size), electrolyte material zinc sulfate (ZnSO_4) and manganese sulfate (MnSO_4), solvent 1,2,4-trichlorobenzene, ethanol and Isoamyl acetate were acquired from Sigma-Aldrich. **Supplementary Figure S1** shows the particle size distribution of the MnO_2 and Mn_3O_4 powder. The particle size of the Mn_3O_4 powder ranges from 1 to $69 \mu\text{m}$ with an average particle size of $11.5 \mu\text{m}$. It is significantly smaller than the particle size of the MnO_2 powder which ranges between 5 and $240 \mu\text{m}$ with an average particle size of $138 \mu\text{m}$. The textile used in this research was a standard fabric used in the clothing industry supplied by Klopman, Italy and was woven from untreated polyester and cotton fibres of ratio 65:35 and diameters of 15 and $12 \mu\text{m}$ respectively. The plain woven textile did not undergo any further treatment. The thickness of the textile was $250 \mu\text{m}$, with 16.5 ends per inch or 9.05 picks per inch and its tensile breaking strength of is 1424 N with a tensile elongation at break of 21.3% based on test method NF EN ISO 13934.

Fabrication Process

The fabrication process of the textile ZIB is shown schematically in **Figure 1A**. The co-polymer solution was prepared by dissolving EVA beads (vinyl acetate 40 wt.%) in 1,2,4-Trichlorobenzene and the PMMA powder in Isoamyl acetate with a ratio between the EVA and PMMA of 7:3 by weight. After both polymer blends were completely dissolved in the solvent, the two polymer solutions were mixed together with a magnetic stirring bar at 60°C (**Figure 1A**). The co-polymer solution was screen printed on top of the polyester-cotton and was then treated with a phase inversion process by immersing the sample in ethanol in a sonicator bath for 20 min before curing the sample under vacuum ($<25 \text{ mBar}$) for 30 min at room temperature. These processes produced a porous co-polymer membrane within the polyester cotton fabrics shown in (**Figure 1B**). This co-polymer membrane acts as the separator of the ZIB which prevents electrical conductivity but allows ion transfer between the anode and cathode.

Following the phase inversion process, the flexible textile ZIB was fabricated using a polymer-composite based flexible anode and cathode which were spray coated on to the flexible co-polymer membrane (**Figure 1A**). These were spray coated on different sides of the textile using a zinc and MnO_2 (or Mn_3O_4) solution respectively. Cathode material solutions contained 5 wt.% of polymer binder, 10 wt.% of carbon black 85 wt.% of amorphous MnO_2 or Mn_3O_4 respectively. The anode solutions contained 3.5 wt.% of polymer binder and 96.5 wt.% of zinc powder. During the spray coating process, both manganese oxides and zinc inks coated and adhered to the unmasked area of the textiles uniformly, with the electrode solutions penetrating the textile substrate. This penetration was limited



and controlled by the polymer membrane, protecting the device from short circuits. The fabrication process for the MnO_2 or Mn_3O_4 cathodes were performed with identical experimental parameters as spray coating time, distance between spray nozzle and substrate, and spray coating pressure. The MnO_2 cathode on the textile has an active material (MnO_2) mass loading of 2.12 mg cm^{-2} and the Mn_3O_4 cathode on the textile has an active material (Mn_3O_4) mass loading of 2.55 mg cm^{-2} . The area of this textile battery is 0.785 cm^2 (i.e., 1 cm diameter) but both solution based processes are suitable for fabricating much larger area devices.

To better understand the electrochemical performance of the two cathode materials, and decouple any effects from the textile device, the MnO_2 , Mn_3O_4 and zinc inks were also spray coated onto separate nickel stainless steel films with identical mass

loading of active materials, shape and area as the textile devices for testing. The reference anode and cathodes on the nickel stainless steel films were sandwiched with a piece of filter paper (grade GF/A from Whatman) to form a ZIB cell. Both the textile ZIB device and the reference battery were vacuum impregnated ($<25 \text{ mBar}$) with the aqueous electrolyte for 30 min at room temperature. The aqueous electrolyte was produced from de-ionized water, 1 M zinc sulfate and 0.1 M manganese sulfate.

Characterization and Electrochemical Testing of Flexible Textile ZIBs

The surface profile and cross-sectional structure of the textile ZIB was obtained by scanning electron microscopy (SEM) using a ZES

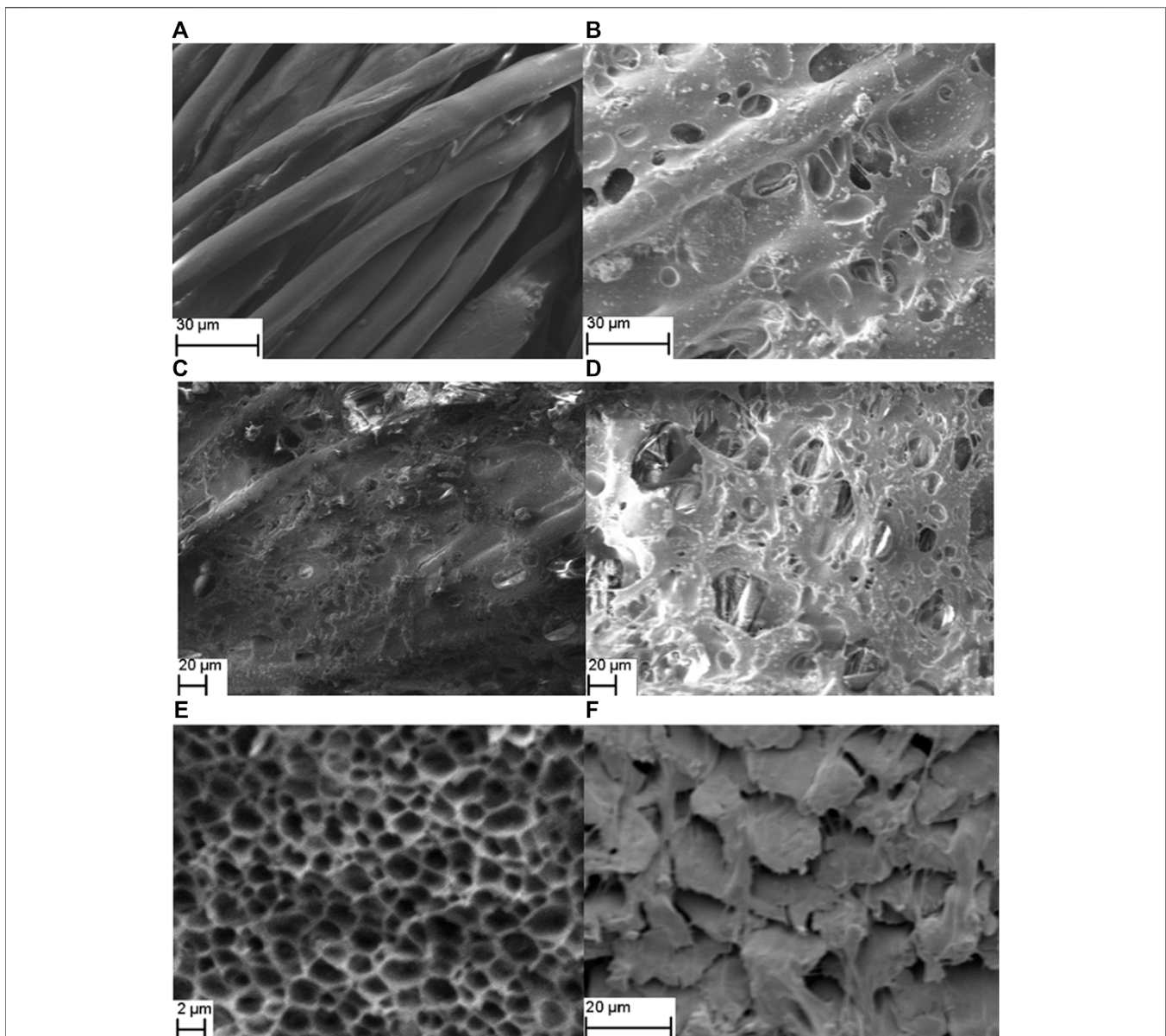
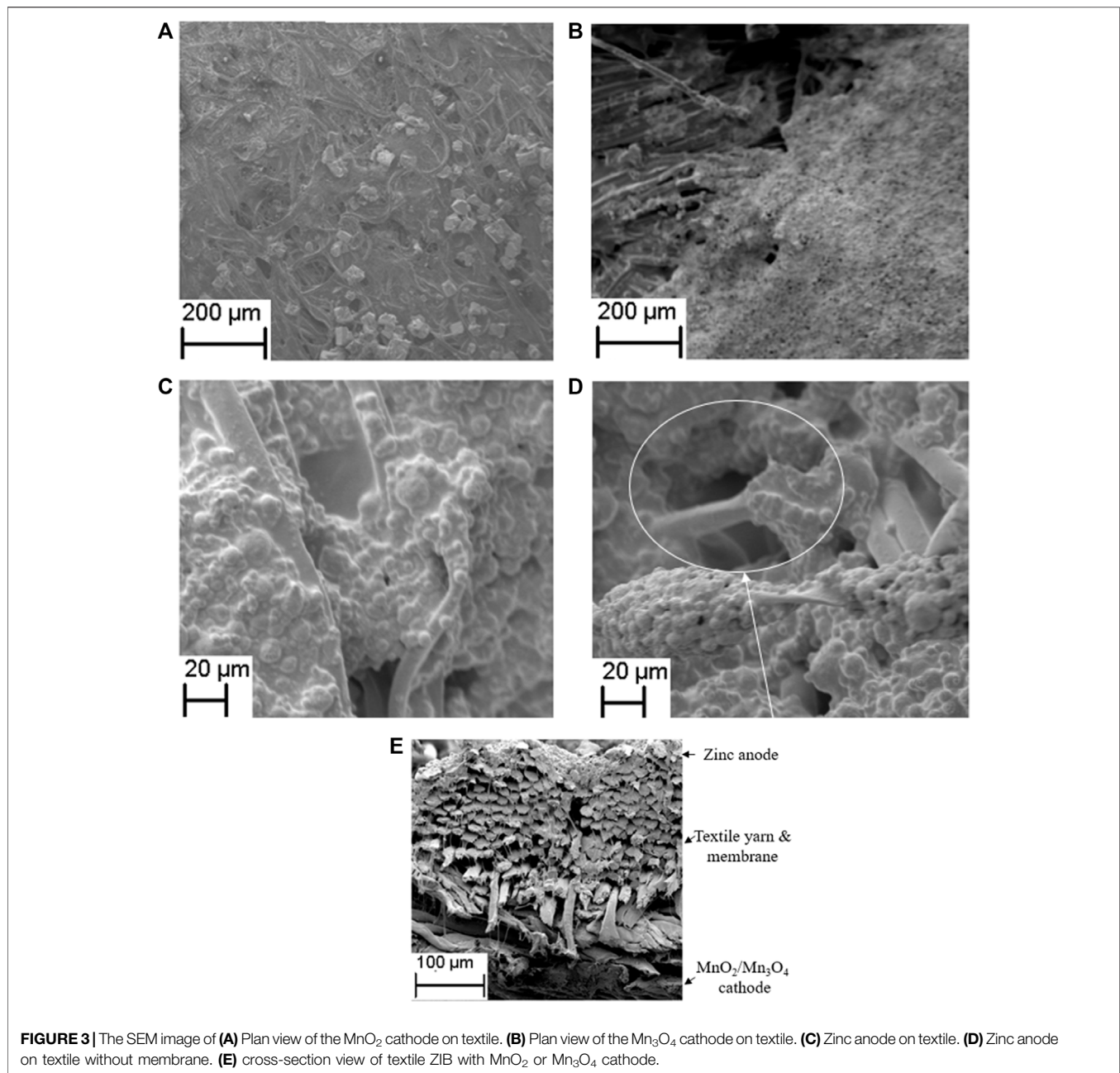


FIGURE 2 | The SEM image of: **(A)** plan view of the polyester cotton textile. **(B)** plan view of textile with polymer membrane. **(C)** plan view of textile with polymer membrane at high magnification. **(D)** cross-section view of textile with polymer membrane. **(E)** plan view of textile with polymer membrane (air dried) without phase inversion at lower magnification. **(F)** plan view of textile with polymer membrane with phase inversion at lower magnification.

EVO microscope at an operating voltage of 5 kV with different magnifications. The particle distribution results of the cathode materials were measured using a Mastersizer 2000 (Malvern, The United Kingdom). The ZIBs were assembled in a two-electrode test system in a Swagelok tube fitting under compression using spring-loaded grade 303 stainless steel current collectors. **Figure 1C** shows the photo of the device test set up and the schematic of the reference ZIB with MnO_2 and Mn_3O_4 cathodes. The electrochemical performance of the reference and textile cells were characterized with the same aqueous electrolyte. The energy storage performance of the reference and textile cells were evaluated using an Autolab PGSTAT101 (Metrohm Autolab,

The Netherlands). Each textile ZIB had a surface area of 0.785 cm^2 with thickness of $\sim 300 \mu\text{m}$. The encapsulated ZIB was characterized by cyclic voltammetry (CV) with a scan rates that vary from 0.625 to 10 mV s^{-1} between 0.9 and 1.9 V , and galvanostatic cycling (GC) at different scan currents (0.5 – 3 mA cm^{-2}) between 0.9 and 1.9 V . The GC results presented are an average from five separate devices. Electrochemical impedance spectroscopy (EIS) was carried out at frequencies varying from 1 Hz to 1 MHz with a peak to peak amplitude of 10 mV in open circuit. The Nyquist plot results from the EIS test were analyzed by Zview software. To evaluate the flexibility of the textile ZIB, several devices were also cyclically

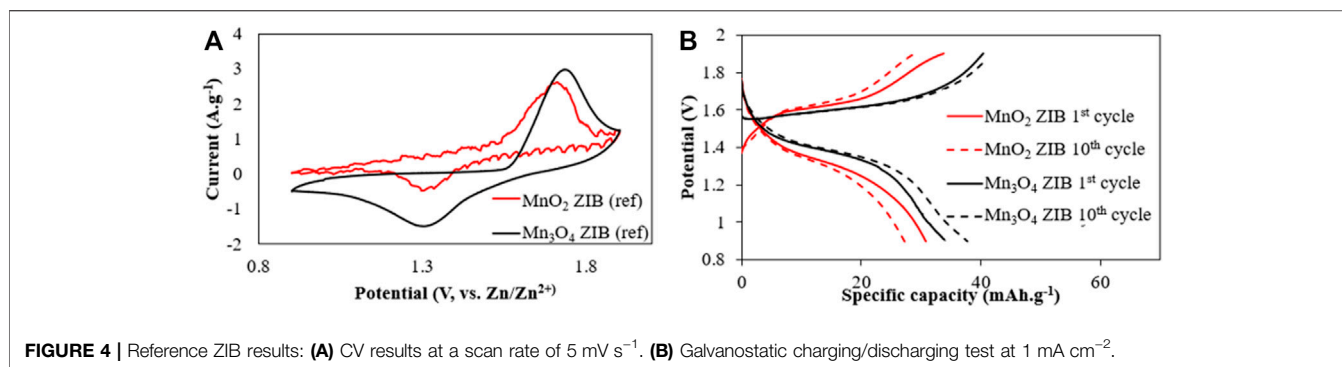


bent around a 3.2 mm diameter mandrel for 2000 cycles at a rate of 2 cycles per second.

RESULT AND DISCUSSION

Figure 2 shows the SEM photos of the polyester-cotton textile before and after the membrane fabrication. The original textile without a membrane clearly shows gaps between the fibers (**Figure 2A**). The porous co-polymer membrane within the textile is shown in **Figure 2B**. The effect of the phase inversion for the creation of porous polymer membrane within the textile are shown in **Figures 2C,D**. The air-dried

polymer membrane (**Figure 2C**) in textile before phase inversion does not show any pore formation and therefore would not allow electrolyte flow through the textile-polymer separator. Following the phase inversion process, the porosity of the membrane is increase (**Figure 2D**) and the membrane develops a polymer lattice, with semi-regular micro pores of around 2 μm which allows good ion mobility (**Figure 2E**). The SEM photograph in **Figure 2F** shows the cross section view of the textile showing the fiber ends covered by the co-polymer indicating the co-polymer is able to penetrate through the fibers in the textile, creating a continuous separator, thus preventing the electrode materials penetrating through the textile and causing short circuits.



As shown in **Figures 3A,B**, after the electrode spray coating process, MnO_2 and Mn_3O_4 particles uniformly coat the textile yarns and co-polymer membrane. The particle size of MnO_2 is significantly larger than Mn_3O_4 . The SEM photos of the zinc anode coating in **Figure 3C** shows that another benefit of the polymer membrane filling the gaps between textile yarns is to reduce the surface roughness of the textile which improves the quality of the zinc coating and which hence forms a continuous and uniformly distributed anode. In **Figure 3D** the textile substrate without the polymer membrane is shown to allow the zinc anode to penetrate through the gaps of the textile yarns. **Figure 3E** shows the SEM image of the cross section view of the textile ZIB with the top (zinc) anode coated yarns and bottom (MnO_2 or Mn_3O_4) cathode coated yarns physically separated by the polymer membrane.

Figure 4A shows the CV test results after the 1st test cycle for the MnO_2 and Mn_3O_4 reference ZIBs. The oxidation (charging) peak of the MnO_2 reference ZIB occurred at 1.71 V , and is smaller and broader than the oxidation (charging) peak of Mn_3O_4 reference ZIB at 1.73 V . Both types of reference ZIBs demonstrated a reduction (discharging) peak at 1.31 V . These are typical voltage peaks for the redox reactions in ZIBs with manganese oxide cathodes (Ming et al., 2019). The reference ZIB with Mn_3O_4 cathode achieved higher peak current value than the ZIB with a MnO_2 cathode, suggesting that the ZIB with a Mn_3O_4 cathode will obtain a higher capacity than the ZIB with a MnO_2 cathode. **Figure 4B** shows the charging and discharging result of the reference ZIB with MnO_2 and Mn_3O_4 cathodes at 1 mA cm^{-2} or 0.3 A g^{-1} . The specific capacity of the reference ZIB with MnO_2 decreased from 30.8 to 27.3 mAh g^{-1} over 10 cycles. This is due to the dissolution of Mn^{2+} which reduces the capacity of the cathode (Sun et al., 2018). The specific capacity of the reference ZIB with Mn_3O_4 increased from 33.9 to 37.7 mAh g^{-1} , this is due to the Mn_3O_4 transforming into MnO_2 (ϵ phase) during the initial cycles (Zhao et al., 2020). This transformation (as detailed in **Eqs 5, 6**) contributes to the overall battery reaction (**Eqs 1–4**) from the 2nd charge-discharge cycle, thus increasing the capacity of the cell. The results in **Figure 4B** agree with the results in **Figure 4A**, showing that the reference ZIB with Mn_3O_4 does achieve a better specific capacity than the identical ZIB with MnO_2 .

The CV plots taken at different scan rates of the textile ZIB (**Figures 5A,B**) demonstrate similar results to the CV plots for the

reference ZIB (**Figure 4A**), with the CV plot of the textile ZIB with the Mn_3O_4 cathode achieving a higher peak current value than the textile ZIB with the MnO_2 cathode. Both devices demonstrated a reduction (discharging) peak at around 1.31 V and an oxidation (charging) peak at around 1.75 V .

Figure 5C shows the charging and discharging results of the textile ZIB with MnO_2 and Mn_3O_4 cathodes at 1 mA cm^{-2} or 0.3 A g^{-1} cycling currents. Both textile ZIBs demonstrated about a third of the specific capacity of the reference ZIBs (**Figure 4B**). This is due to the difference between the textile membrane and the filter paper based separator. The filter paper is thinner, increasing the ionic conductivity and has improved wettability characteristics. In the textile integrated polymer separator, these two properties can be improved *via* the use of thinner textile (such as silk) to reduce the overall thickness, textile with natural fibers, change the membrane's polymer composition or optimize the material ratio and fabrication process of the polymer membrane. The textile ZIB with the Mn_3O_4 cathode achieved an initial specific capacity of 10.9 mAh g^{-1} (1st cycle) which increased to 11.5 mAh g^{-1} (10th cycles) because of the transformation of Mn_3O_4 to MnO_2 as previously discussed. This is higher than the specific capacity of the textile ZIB with the amorphous MnO_2 cathode of 8.95 mAh g^{-1} (1st cycle) which decreased to 7.15 mAh g^{-1} after 10 test cycles. As previously reported, amorphous MnO_2 material has a theoretic capacity of 308 mAh g^{-1} (Wang R. et al., 2022), however, its low electrical conductivity and large particle size limit its performance. The superior performance of the Mn_3O_4 cathode compared with the MnO_2 cathode was further confirmed by the rate capability test results shown in **Figure 5D**. The specific capacity variation of the textile ZIB with MnO_2 and Mn_3O_4 cathodes were measured at four current densities $1, 1.5, 2$ and 3 mA cm^{-2} or $0.3, 0.45, 0.6$ and 0.9 A g^{-1} . The textile ZIB with the Mn_3O_4 cathode exhibited higher average specific capacities of $10.9, 4.76, 2.48,$ and 0.77 mAh g^{-1} compared to the textile ZIB with MnO_2 ($8.95, 3.5, 0.72,$ and 0.1 mAh g^{-1}).

From **Figure 5E**, the maximum energy density and average power density of the textile ZIB with the Mn_3O_4 cathode and MnO_2 cathode obtained at a cycling current of 1 mA cm^{-2} or 0.3 A g^{-1} were 13.2 mWh.g^{-1} or 374 mW g^{-1} and 8.64 mWh.g^{-1} or 362 mW g^{-1} respectively. An increase in the cycling current to 3 mA cm^{-2} or 0.9 A g^{-1} results in an increase in average power density to $1,161 \text{ mW g}^{-1}$ for the textile ZIB with Mn_3O_4 cathode.

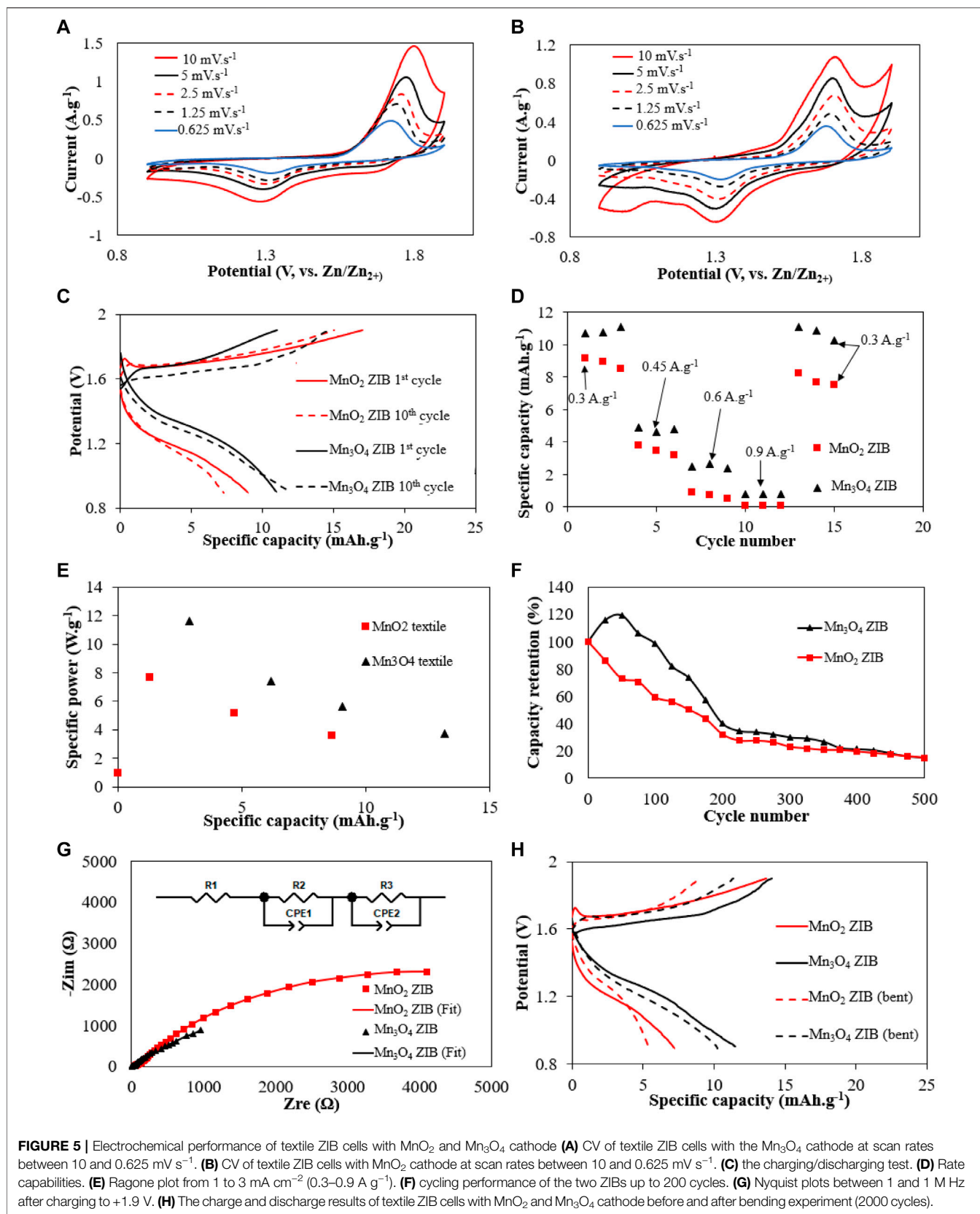


FIGURE 5 | Electrochemical performance of textile ZIB cells with MnO_2 and Mn_3O_4 cathode (A) CV of textile ZIB cells with the Mn_3O_4 cathode at scan rates between 10 and 0.625 mV s^{-1} . (B) CV of textile ZIB cells with MnO_2 cathode at scan rates between 10 and 0.625 mV s^{-1} . (C) the charging/discharging test. (D) Rate capabilities. (E) Ragone plot from 1 to 3 mA cm^{-2} ($0.3\text{--}0.9 \text{ A g}^{-1}$). (F) cycling performance of the two ZIBs up to 200 cycles. (G) Nyquist plots between 1 and 1 MHz after charging to $+1.9 \text{ V}$. (H) The charge and discharge results of textile ZIB cells with MnO_2 and Mn_3O_4 cathode before and after bending experiment (2000 cycles).

TABLE 1 | EIS fitting result of textile ZIB with MnO₂ and Mn₃O₄ cathode.

(Ω)	R1	R2	R3
MnO ₂	24.1	313.9	1813
Mn ₃ O ₄	4.38	25.6	1787

The textile ZIB with MnO₂ cathode failed at a cycling current of 0.9 A g⁻¹ due to the MnO₂ material having higher impedance than the Mn₃O₄ device (**Figure 5G**). When testing the ZIB at 0.9 A g⁻¹, the losses from the higher impedance results in a large initial voltage drop, taking the device below the safe operating voltage (0.9 V) and immediately terminating the test. The results of cycling stability test are shown in **Figure 5F**. The capacity of the textile ZIB with Mn₃O₄ cathode increased over the first 20 cycles, due to the Mn₃O₄ transformation to MnO₂. The capacity of the textile ZIB with Mn₃O₄ cathode decreased by 5% after 100 cycles, whereas the textile ZIB with MnO₂ cathode only retained 60% of its initial capacity. After 200 cycles the capacity of both textile ZIBs reduced to approximately 40% of its original value. The capacity of both textile ZIBs dropped below 15% after 500 cycles. The capacity reduction of textile ZIB with both MnO₂ and Mn₃O₄ cathode correlates to the dissolution of Mn²⁺ ions (the Jahn-Teller effect) from the cathode materials into the electrolyte, varying the concentration of the Mn⁴⁺ and Mn³⁺ ions in the electrolyte, and thus changing the electrolyte's PH level from mild acidic to neutral. This induces the formation of Zn-birnessite (Zn₅MnO₂) when the Zn ions intercalate into the cathode. The Zn-birnessite is not electrochemically active in this system and results in capacity fade of the ZIB over time (Lee et al., 2014). This justifies the addition of 0.1 M MnSO₄ salt into the electrolyte to accommodate the dissolution equilibrium of Mn²⁺ (Ming et al., 2019).

The EIS test results, equivalent circuit and fitted results of the textile ZIB with MnO₂ and Mn₃O₄ cathode are shown in **Figure 5G**. In the equivalent circuit (insert in **Figure 5G**), R1 represents the ohmic series resistance, R2 represents the surface film resistance and R3 represents the charge transfer resistance (Shen et al., 2021). According to **Table 1** all three resistance values of the textile ZIB with Mn₃O₄ were lower than the textile ZIB with MnO₂, leading to less loss and higher energy storage capacity at increasing current densities, as shown in **Figure 5D**.

Figure 5H shows the GC test result (0.3 A g⁻¹ or 1 mA cm⁻²) of the textile ZIB and after mechanically bending the textile ZIB 2000 times around a 3.2 mm diameter mandrel. The textile ZIB with the Mn₃O₄ cathode demonstrated a lower capacity loss of 12% (from 11.5 to 10.12 mAh g⁻¹) whereas the textile ZIB with MnO₂ cathode exhibited a reduction in capacity of 24% (from 7.15 to 5.43 mAh g⁻¹). The textile ZIB with Mn₃O₄ cathode also achieved a lower energy density loss of 2.92% (from 13.2 to 12.8 mWh g⁻¹) whereas the textile ZIB with MnO₂ cathode exhibited higher capacity loss of 3.86% (from 8.64 to 8.31 mWh g⁻¹). These indicate the textile ZIB is not critically affected by the application of repeated mechanical bending strains. The textile ZIB with the Mn₃O₄ cathode demonstrated better resistance to cyclical mechanical

bending strains with less capacity loss than the textile ZIB with MnO₂ cathode. This is understood to be due to the smaller particle size of the Mn₃O₄ forming a better conductive network within the electrode than the larger MnO₂ particles. Upon bending, the electrode will experience micro cracking, resulting in separation of the active material. For the well distributed Mn₃O₄ this is not significant as there remains a good electrical network in spite of any micro cracking. The MnO₂ conductive network, on the other hand, is far less resilient to the cracking due to the larger particles separating from each other (and the carbon filler) and possibly the textile. The results relating to the reduction in capacity are comparable with other devices in the literature. Sun et al (Sun et al., 2022) demonstrated a flexible zinc ion battery with aqueous electrolyte which maintained 90% of its original capacity after a series of angular bending for 100 cycles. Yan et al. (Yan et al., 2021) implemented a flexible aqueous zinc ion battery and achieved capacity retention of 83% after 80 bending cycles.

CONCLUSION

This work has demonstrated for the first time the capability of integrating a zinc ion battery with manganese-based cathode within a single piece of polyester-cotton textile. The electrochemical performance of the single textile ZIB with commercially available amorphous MnO₂ and Mn₃O₄ material as the cathode has been experimentally characterised. Both textile ZIBs achieved a working voltage range of 1.9 and 0.9 V. The textile ZIB with Mn₃O₄ cathode achieved higher capacity (10.9 mAh g⁻¹ at 0.3 A g⁻¹) than the textile ZIB with the MnO₂ cathode. The textile ZIB with Mn₃O₄ cathode also retained over 95% of capacity after 100 cycles whereas the textile ZIB with the MnO₂ cathode only kept around 60% of its capacity after 100 cycles. The fact the electrochemical results of the textile ZIB shown are not as good as the reference ZIB indicates further work is required to improve ionic conductivity and wettability of the membrane. This will involve further investigating the influence of different polymers used in the membrane fabrication in order to increase the level of porosity and improve wettability. The PMMA/EVA porous layer in the textile successfully separated the MnO₂/Mn₃O₄ and zinc and allowed for a uniform deposition of the electrodes. The vacuum impregnation process ensured the aqueous electrolyte filled the membrane layer and wetted both the anode and cathode materials. In comparison with other works, these results were not as good as previous multilayer ZIB with synthesized MnO₂ cathode and individual separator layer. However, in this work, the anode, cathode and separator layer were integrated into a single layer of polyester cotton textile using scalable and inexpensive processes and this presents a reliable approach for realizing an energy storage device in textiles for e-textile applications. Future work will include optimizing the ZIB's encapsulation material/method to achieve a well-sealed, flexible and washable device, improving the porosity and structure of the separator, investigating the particle size distribution of the anode/cathode material powders *via* milling, optimizing formulations of the anode/cathode inks and electrolyte

to increase the flexible ZIB electrochemical performance. Further investigations of device reliability such as its ability to withstand machine washing will be completed once device encapsulation has been fully investigated. The final device could be used to power future devices in a wide range of e-textile systems.

DATA AVAILABILITY STATEMENT

The original contributions presented in the study are included in the article/**Supplementary Material**, further inquiries can be directed to the corresponding author.

AUTHOR CONTRIBUTIONS

SY: Conceptualization, Methodology, Validation, Formal analysis, Investigation, Data curation, Writing—original draft, Writing—review and editing, Visualization. NH: Formal analysis, Validation, Writing—original draft, Writing—review and

REFERENCES

- Atalay, O., Kalaoglu, F., and Kursun Bahadir, S. (2019). Development of Textile-Based Transmission Lines Using Conductive Yarns and Ultrasonic Welding Technology for E-Textile Applications. *J. Eng. Fibers Fabr.* 14, 155892501985660. doi:10.1177/1558925019856603
- Chen, H., Zhou, W., Zhu, D., Liu, Z., Feng, Z., Li, J., et al. (2020). Porous Cube-Like Mn₃O₄@C as an Advanced Cathode for Low-Cost Neutral Zinc-Ion Battery. *J. Alloys Compd.* 813, 151812. doi:10.1016/j.jallcom.2019.151812
- Chen, Y., Kang, Y., Zhao, Y., Wang, L., Liu, J., Li, Y., et al. (2021). A Review of Lithium-Ion Battery Safety Concerns: The Issues, Strategies, and Testing Standards. *J. Energy Chem.* 59, 83–99. doi:10.1016/j.jechem.2020.10.017
- Cinquino, M., Prontera, C., Pugliese, M., Giannuzzi, R., Taurino, D., Gigli, G., et al. (2021). Light-Emitting Textiles: Device Architectures, Working Principles, and Applications. *Micromachines* 12 (6), 652. doi:10.3390/mi12060652
- Cleary, F., Henshall, D. C., and Balasbramian, S. (2021). On-Body Edge Computing Through E-Textile Programmable Logic Array. *Front. Comms. Net.* 2, 688419. doi:10.3389/frcmn.2021.688419
- Fakharuddin, A., Li, H., Di Giacomo, F., Zhang, T., Gasparini, N., Elezzabi, A. Y., et al. (2021). Fiber-Shaped Electronic Devices. *Adv. Energy Mat.* 11 (34), 2101443. doi:10.1002/aenm.202101443
- Fromme, N. P., Li, Y., Camenzind, M., Toncelli, C., and Rossi, R. M. (2021). Metal-Textile Laser Welding for Wearable Sensors Applications. *Adv. Electron. Mat.* 7 (4), 2001238. doi:10.1002/aelm.202001238
- Hao, J., Mou, J., Zhang, J., Dong, L., Liu, W., Xu, C., et al. (2018). Electrochemically Induced Spinel-Layered Phase Transition of Mn₃O₄ in High Performance Neutral Aqueous Rechargeable Zinc Battery. *Electrochimica Acta* 259, 170–178. doi:10.1016/j.electacta.2017.10.166
- Huang, Y., Liu, J., Zhang, J., Jin, S., Jiang, Y., Zhang, S., et al. (2019). Flexible Quasi-Solid-State Zinc Ion Batteries Enabled by Highly Conductive Carrageenan Bio-Polymer Electrolyte. *RSC Adv.* 9 (29), 16313–16319. doi:10.1039/c9ra01120j
- Jang, J., Oh, J., Jeong, H., Kang, W., and Jo, C. (2020). A Review of Functional Separators for Lithium Metal Battery Applications. *Materials* 13 (20), 4625. doi:10.3390/ma13204625
- Javed, M. S., Lei, H., Wang, Z., Liu, B.-t., Cai, X., and Mai, W. (2020). 2D V₂O₅ Nanosheets as a Binder-Free High-Energy Cathode for Ultrafast Aqueous and Flexible Zn-Ion Batteries. *Nano Energy* 70, 104573. doi:10.1016/j.nanoen.2020.104573
- Jiao, Y., Kang, L., Berry-Gair, J., McColl, K., Li, J., Dong, H., et al. (2020). Enabling Stable MnO₂ Matrix for Aqueous Zinc-Ion Battery Cathodes. *J. Mat. Chem. A* 8 (42), 22075–22082. doi:10.1039/d0ta08638j

editing. SB: Resources, Writing—review and editing, Supervision, Funding acquisition, Project administration.

FUNDING

This research was funded and supported by United State Army with Contract No: W911NF2010324 and EPSRC Grants EP/P010164/1 and EP/L016818/1. The work of SB was supported by the Royal Academy of Engineering under the Chairs in Emerging Technologies Scheme.

SUPPLEMENTARY MATERIAL

The Supplementary Material for this article can be found online at: <https://www.frontiersin.org/articles/10.3389/felec.2022.866527/full#supplementary-material>

- Jin, Y., Han, K. S., Shao, Y., Sushko, M. L., Xiao, J., Pan, H., et al. (2020). Stabilizing Zinc Anode Reactions by Polyethylene Oxide Polymer in Mild Aqueous Electrolytes. *Adv. Funct. Mat.* 30 (43), 2003932. doi:10.1002/adfm.202003932
- Komolafe, A., Torah, R., Wei, Y., Nunes-Matos, H., Li, M., Hardy, D., et al. (2019). Integrating Flexible Filament Circuits for E-Textile Applications. *Adv. Mat. Technol.* 4 (7), 1900176. doi:10.1002/admt.201900176
- Komolafe, A., Zaghari, B., Torah, R., Weddell, A. S., Khanbareh, H., Tsikriteas, Z. M., et al. (2021). E-Textile Technology Review-From Materials to Application. *IEEE Access* 9, 97152–97179. doi:10.1109/Access.2021.3094303
- Lahmann, N. A., Müller-Werdan, U., Kuntz, S., Klingehöfer-Noe, J., Jaenicke, F., and Strube-Lahmann, S. (2022). Conception and Evaluation of a Washable Multimodal Smart Textile. *Health Technol.* 12 (1), 69–81. doi:10.1007/s12553-021-00619-6
- Lee, B.-S., Cui, S., Xing, X., Liu, H., Yue, X., Petrova, V., et al. (2018). Dendrite Suppression Membranes for Rechargeable Zinc Batteries. *ACS Appl. Mat. Interfaces* 10 (45), 38928–38935. doi:10.1021/acsami.8b14022
- Lee, B., Yoon, C. S., Lee, H. R., Chung, K. Y., Cho, B. W., and Oh, S. H. (2014). Electrochemically-Induced Reversible Transition from the Tunneled to Layered Polymorphs of Manganese Dioxide. *Sci. Rep.* 4, 6066. doi:10.1038/srep06066
- Liu, X., Ren, D., Hsu, H., Feng, X., Xu, G.-L., Zhuang, M., et al. (2018). Thermal Runaway of Lithium-Ion Batteries without Internal Short Circuit. *Joule* 2 (10), 2047–2064. doi:10.1016/j.joule.2018.06.015
- Mauriello, M. L., Gubbels, M., and Froehlich, J. E. (2014). “Social Fabric Fitness: The Design and Evaluation of Wearable E-Textile Displays to Support Group Running,” in 32nd Annual Acm Conference on Human Factors in Computing Systems (Chi 2014), 2833–2842. doi:10.1145/2556288.2557299
- Ming, J., Guo, J., Xia, C., Wang, W., and Alshareef, H. N. (2019). Zinc-ion Batteries: Materials, Mechanisms, and Applications. *Mater. Sci. Eng. R Rep.* 135, 58–84. doi:10.1016/j.mser.2018.10.002
- Peppler, K., and Glosson, D. (2013). Stitching Circuits: Learning about Circuitry through E-Textile Materials. *J. Sci. Educ. Technol.* 22 (5), 751–763. doi:10.1007/s10956-012-9428-2
- Pu, X., Li, L., Song, H., Du, C., Zhao, Z., Jiang, C., et al. (2015). A Self-Charging Power Unit by Integration of a Textile Triboelectric Nanogenerator and a Flexible Lithium-Ion Battery for Wearable Electronics. *Adv. Mat.* 27 (15), 2472–2478. doi:10.1002/adma.201500311
- Qian, X., Qiu, R., Lu, C., Qiu, Y., Wu, Z., Wang, S., et al. (2020). Cost-Effective Yarn-Shaped Lithium-Ion Battery with High Wearability. *ACS Omega* 5 (9), 4697–4704. doi:10.1021/acsomega.0c00254
- Selvakumaran, D., Pan, A., Liang, S., and Cao, G. (2019). A Review on Recent Developments and Challenges of Cathode Materials for Rechargeable Aqueous Zn-Ion Batteries. *J. Mat. Chem. A* 7 (31), 18209–18236. doi:10.1039/c9ta05053a

- Shen, H., Liu, B., Nie, Z., Li, Z., Jin, S., Huang, Y., et al. (2021). A Comparison Study of MnO₂ and Mn₂O₃ as Zinc-Ion Battery Cathodes: an Experimental and Computational Investigation. *RSC Adv.* 11 (24), 14408–14414. doi:10.1039/d1ra00346a
- Shi, X., Zuo, Y., Zhai, P., Shen, J., Yang, Y., Gao, Z., et al. (2021). Large-Area Display Textiles Integrated with Functional Systems. *Nature* 591 (7849), 240–245. doi:10.1038/s41586-021-03295-8
- Somov, A., Alonso, E. T., Craciun, M. F., Neves, A. I. S., and Baldycheva, A. (2017). “Smart Textile: Exploration of Wireless Sensing Capabilities,” in 2017 IEEE Sensors, Glasgow, UK, 29 Oct.-1 Nov. 2017, 546–548. doi:10.1109/icsens.2017.8234058
- Sun, G., Jin, X., Yang, H., Gao, J., and Qu, L. (2018). An Aqueous Zn-MnO₂ Rechargeable Microbattery. *J. Mat. Chem. A* 6 (23), 10926–10931. doi:10.1039/c8ta02747a
- Sun, G., Yang, B., Chen, X., Wei, Y., Yin, G., Zhang, H., et al. (2022). Aqueous Zinc Batteries Using N-Containing Organic Cathodes with Zn²⁺ and H⁺ Co-Uptake. *Chem. Eng. J.* 431 (3), 134253. doi:10.1016/j.cej.2021.134253
- Sun, Q., Bijelić, M., Djurišić, A. B., Suchomski, C., Liu, X., Xie, M., et al. (2017). Graphene-Oxide-Wrapped ZnMn₂O₄ as a High Performance Lithium-Ion Battery Anode. *Nanotechnology* 28 (45), 455401. doi:10.1088/1361-6528/aa8a5b
- Wang, F., Borodin, O., Gao, T., Fan, X., Sun, W., Han, F., et al. (2018a). Highly Reversible Zinc Metal Anode for Aqueous Batteries. *Nat. Mater* 17 (6), 543–549. doi:10.1038/s41563-018-0063-z
- Wang, L., Cao, X., Xu, L., Chen, J., and Zheng, J. (2018b). Transformed Akhtenskite MnO₂ from Mn₃O₄ as Cathode for a Rechargeable Aqueous Zinc Ion Battery. *ACS Sustain. Chem. Eng.* 6 (12), 16055–16063. doi:10.1021/acsschemeng.8b02502
- Wang, R., Liu, Z., Zhao, D., Xu, J., Cao, Y., Huang, J., et al. (2022a). *In Situ* micro-current Collector of Amorphous Manganese Dioxide as Cathode Material for Sodium-Ion Batteries. *Ionics* 28, 1211–1217. doi:10.1007/s11581-021-04403-4
- Wang, S., Xu, Q., and Sun, H. (2022b). Functionalization of Fiber Devices: Materials, Preparations and Applications. *Adv. Fiber Mat.* 4, 324–341. doi:10.1007/s42765-021-00120-9
- Wang, Y., Peng, H., Hu, M., Zhuang, L., Lu, J., and Xiao, L. (2021). A Stable Zinc-Based Secondary Battery Realized by Anion-Exchange Membrane as the Separator. *J. Power Sources* 486, 229376. doi:10.1016/j.jpowsour.2020.229376
- Wicaksono, I., Tucker, C. I., Sun, T., Guerrero, C. A., Liu, C., Woo, W. M., et al. (2020). A Tailored, Electronic Textile Conformable Suit for Large-Scale Spatiotemporal Physiological Sensing *In Vivo*. *npj Flex. Electron* 4 (1), 5. doi:10.1038/s41528-020-0068-y
- Wu, X., Song, K., Zhang, X., Hu, N., Li, L., Li, W., et al. (2019). Safety Issues in Lithium Ion Batteries: Materials and Cell Design. *Front. Energy Res.* 7, 65. doi:10.3389/fenrg.2019.00065
- Yan, L., Zhang, Y., Ni, Z., Zhang, Y., Xu, J., Kong, T., et al. (2021). Chemically Self-Charging Aqueous Zinc-Organic Battery. *J. Am. Chem. Soc.* 143 (37), 15369–15377. doi:10.1021/jacs.1c06936
- Yao, D. J., Tang, Z. H., Zhang, L., Li, R. L., Zhang, Y. Z., Zeng, H. X., et al. (2021). Gas-Permeable and Highly Sensitive, Washable and Wearable Strain Sensors Based on Graphene/Carbon Nanotubes Hybrids E-Textile. *Compos. Part A-Appl. Sci. Manuf.* 149, 106556. doi:10.1016/j.compositesa.2021.106556
- Yong, S., Owen, J., and Beeby, S. (2018). Solid-State Supercapacitor Fabricated in a Single Woven Textile Layer for E-Textiles Applications. *Adv. Eng. Mat.* 20 (5), 1700860. doi:10.1002/adem.201700860
- Yong, S., Hillier, N., Yang, K., and Beeby, S. (2019). Integrated Flexible Textile Supercapacitor Fabricated in a Polyester-Cotton Fabric. *Proceedings* 32 (15). doi:10.3390/proceedings2019032015
- Zhang, W., Tu, Z., Qian, J., Choudhury, S., Archer, L. A., and Lu, Y. (2018). Design Principles of Functional Polymer Separators for High-Energy, Metal-Based Batteries. *Small* 14 (11), 1703001. doi:10.1002/sml.201703001
- Zhao, J., and Burke, A. F. (2021). Review on Supercapacitors: Technologies and Performance Evaluation. *J. Energy Chem.* 59, 276–291. doi:10.1016/j.jechem.2020.11.013
- Zhao, Q., Huang, W., Luo, Z., Liu, L., Lu, Y., Li, Y., et al. (2018). High-Capacity Aqueous Zinc Batteries Using Sustainable Quinone Electrodes. *Sci. Adv.* 4 (3), eaao1761. doi:10.1126/sciadv.aao1761
- Zhao, Y., Zhu, Y., and Zhang, X. (2020). Challenges and Perspectives for Manganese-Based Oxides for Advanced Aqueous Zinc-ion Batteries. *Infomat* 2 (2), 237–260. doi:10.1002/inf.2.12042

Conflict of Interest: The authors declare that the research was conducted in the absence of any commercial or financial relationships that could be construed as a potential conflict of interest.

Publisher’s Note: All claims expressed in this article are solely those of the authors and do not necessarily represent those of their affiliated organizations, or those of the publisher, the editors and the reviewers. Any product that may be evaluated in this article, or claim that may be made by its manufacturer, is not guaranteed or endorsed by the publisher.

Copyright © 2022 Yong, Hillier and Beeby. This is an open-access article distributed under the terms of the Creative Commons Attribution License (CC BY). The use, distribution or reproduction in other forums is permitted, provided the original author(s) and the copyright owner(s) are credited and that the original publication in this journal is cited, in accordance with accepted academic practice. No use, distribution or reproduction is permitted which does not comply with these terms.